



LAWRENCE
LIVERMORE
NATIONAL
LABORATORY

Compton scattering overview

F. V. Hartemann

December 24, 2008

Compton Sources for X/gamma Rays: Physics & Apps
Alghero, Italy
September 5, 2008 through September 13, 2008

Disclaimer

This document was prepared as an account of work sponsored by an agency of the United States government. Neither the United States government nor Lawrence Livermore National Security, LLC, nor any of their employees makes any warranty, expressed or implied, or assumes any legal liability or responsibility for the accuracy, completeness, or usefulness of any information, apparatus, product, or process disclosed, or represents that its use would not infringe privately owned rights. Reference herein to any specific commercial product, process, or service by trade name, trademark, manufacturer, or otherwise does not necessarily constitute or imply its endorsement, recommendation, or favoring by the United States government or Lawrence Livermore National Security, LLC. The views and opinions of authors expressed herein do not necessarily state or reflect those of the United States government or Lawrence Livermore National Security, LLC, and shall not be used for advertising or product endorsement purposes.

Compton scattering overview

F.V. Hartemann

Lawrence Livermore National Laboratory, Livermore, CA 94550

This work performed under the auspices of the U.S. Department of Energy by Lawrence Livermore National Laboratory under Contract DE-AC52-07NA27344.

Abstract

An overview of linear and nonlinear Compton scattering is presented, along with a comparison with Thomson scattering. Two distinct processes play important roles in the nonlinear regime: multi-photon interactions, leading to the generation of harmonics, and radiation pressure, yielding a downshift of the radiated spectral features. These mechanisms, their influence on the source brightness, and different modeling strategies are also briefly discussed.

1. Introduction

The main goal of this paper is to provide a brief overview of Compton scattering [1-5], both in the linear and nonlinear regimes, along with a comparison of these processes with Thomson scattering. Since our intent is to understand the physical mechanisms underlying the radiation characteristics of relativistic electrons subjected to intense laser pulses, plane wave models will be used, although three-dimensional effects are also outlined.

The motivation behind this work is threefold: first, linear and nonlinear Thomson and Compton scattering are fundamental processes in classical and quantum electrodynamics, and involve a wealth of important physical mechanisms, including harmonic production, multi-photon interactions, and the dynamics of dressed electrons in a coherent electromagnetic field; second, a number of key applications of Compton scattering light sources require very narrow band operation; nuclear resonance fluorescence (NRF) [6], and multi-wavelength anomalous dispersion (MAD) in x-ray protein crystallography [7] are two such examples; finally, appropriate space-time shaping and optimization of the laser electromagnetic wiggler can lead to enhanced spectral brightness. Therefore, such mechanisms should be accounted for in the design of these novel radiation sources, and spectral broadening mitigation strategies should cover both linear, nonlinear, and three-dimensional effects: for example, both the inhomogeneous radiation pressure in an intense laser pulse and the generation of harmonics can lead to a decrease of the source spectral brightness, while electron beam and laser pulse phase-space correlations also contribute to the output radiation characteristics.

This paper is organized as follows: basic scaling laws and spectral broadening effects are first discussed in Section 2, along with different modeling approaches; in Section 3, the nonlinear electron dynamics are reviewed, and nonlinear Compton and Thomson scattering are presented and compared; the key physical mechanisms underlying harmonic production and ponderomotive downshift are identified; finally, conclusions are drawn in Section 4.

2. Scaling, spectral broadening mechanisms

Two fundamental scales characterize the strength of electromagnetic fields: the normalized vector potential, $A_0 = e\sqrt{-A_\mu A^\mu} / m_0 c$, which measures the potential in classical electron units; and the Schwinger critical field, $E_s = m_0^2 c^3 / e\hbar$, which is related to the probability of tunneling electron-positron pairs from the QED vacuum. The strength of the normalized vector potential, which can be connected to the local photon density via the relation $A_0^2 = 2n_\lambda r_0 \hat{\lambda}_c \lambda$, governs the nonlinear dynamics of electrons in electromagnetic fields: the onset of relativistic transverse motion, ponderomotive effects, and harmonic radiation are all scaling with A_0 . In the above, $r_0 = e^2 / 4\pi\epsilon_0 m_0 c^2$ is the classical electron radius, $\hat{\lambda}_c = \hbar / m_0 c = r_0 / \alpha$ is the Compton wavelength of the electron, α is the fine structure constant, and λ is the wavelength of the electromagnetic radiation.

This section is intended as a cursory review of known properties of Thomson and Compton scattering; for details, we refer the reader to References [1-5]. As will be shown in Section 3, the Compton formula provides a relation between the frequency of

the scattered radiation and the electron initial 4-velocity, the incident radiation 4-wavenumber, and the direction of observation; in the nonlinear case, a harmonic number also characterizes the scattered radiation:

$$q_m = m \frac{\gamma k - \mathbf{u} \cdot \mathbf{k}}{\gamma - \mathbf{u} \cdot \mathbf{n} - \frac{\langle A_v A^v \rangle}{2} \left(\frac{k - \mathbf{k} \cdot \mathbf{n}}{\gamma k - \mathbf{u} \cdot \mathbf{k}} \right) + \tilde{\lambda}_c m (k - \mathbf{k} \cdot \mathbf{n})}. \quad (1)$$

Here, m is the harmonic number, $k_\mu = (k, \mathbf{k})$ is the incident 4-wavenumber, $u_\mu = (\gamma, \mathbf{u})$ is the electron 4-velocity before the interaction, and \mathbf{n} is the direction of observation, which is related to the scattered 4-wavenumber via $q_\mu = q(1, \mathbf{n})$. The average of the square of the normalized vector potential appears, describing the ponderomotive downshift of the radiation; the factor of $\frac{1}{2}$ corresponds to linear polarization.

A number of important characteristics of Compton scattering can be directly deduced from the structure of Equation (1); in particular, spectral broadening mechanisms can be clearly identified. First, the relativistic Doppler upshift shows that the scattered radiation depends sensitively upon the electron beam phase space: the energy spread, $\Delta\gamma / \gamma$; normalized emittance, ε_n ; focal spot size, σ_b ; and beam pointing stability; all contribute to the width of the radiation produced by the source. Next, the incident laser pulse phase space, related to the Wigner distribution function [8,9], play an important role via the relative spectral bandwidth, $\Delta k / k$; the f -number and M^2 , as well as correlations, including spatial or temporal chirps. Finally, recoil, multiple collisions, inhomogeneous radiation pressure, and harmonic production can all lead to spectral broadening.

Beyond the Compton formula, the Klein-Nishina differential scattering cross-section [5] provides the appropriate scattering amplitude for linear processes; in the nonlinear case, a complete, self-consistent, three-dimensional theory that can fully incorporate electron beam and laser pulse phase space correlations is still lacking, but a number of approaches, complementary in nature, can be followed to provide sufficient information. To conclude this section, we list a few theory and modeling strategies; roughly speaking, these fall into four main categories: plane wave models and three-dimensional theories; and particle versus wave models. The simplest approach consists in using the Lorentz force equation to describe the electron dynamics, coupled to the radiation formula [10], thus describing linear Thomson scattering; linear Compton scattering can be modeled by using the Klein-Nishina differential scattering cross-section and the Compton formula; three-dimensional effects can be added by considering incoherent summations over the electron beam phase space, along with electromagnetic field models, such as the paraxial approximation or Gaussian-Hermite modes. We also note that the addition of an *ad-hoc* recoil-like term to the electron dynamics can be used to model recoil within the Thomson formalism. Nonlinear effects, while easily described in classical (Thomson), or semi-classical terms, are more difficult to handle via the scattering cross-section formalism, and require the introduction of multi-photon cross-sections together with multiple incident phase space integrations. In terms of wave and particle models, one can first consider the radiation formula: the electron motion is Fourier transformed over time; chirp and other laser correlations can be accounted for, and nonlinear effects can be included straightforwardly; however, neither recoil (both in frequency and cross-section), nor spin are described. Using the

differential cross-section, on the other hand, allows for the retrieval of temporal information, and accounts for recoil and spin. Within this context, correlated laser phase spaces require using the Wigner distribution approach, and nonlinear effects are much more difficult to implement.

Finally, we also note that Monte-Carlo simulations offer a powerful alternative approach to describing three-dimensional and nonlinear effects, although one important challenge remains the appropriate mapping of the incident electromagnetic field distribution onto the corresponding photon phase space.

3. Nonlinear effects

In this section, the nonlinear Thomson and Compton scattering spectral characteristics are compared for a linearly polarized plane wave in an arbitrary frame.

The electron 4-velocity satisfies the Lorentz force equation;

$$u_{\mu} = u_{\mu}^0 + A_{\mu} - k_{\mu} \frac{A_{\nu} A^{\nu} + 2u_{\nu}^0 A^{\nu}}{2u_{\nu}^0 k^{\nu}}, \quad (2)$$

where u_{μ}^0 is the electron 4-velocity before (and after) the interaction; $A_{\mu} = \varepsilon_{\mu} A_0 \sin \phi$ is the 4-potential of the plane wave expressed in terms of its 4-polarization, ε_{μ} , normalized amplitude, A_0 , and phase $\phi = k_{\mu} x^{\mu}$; k_{μ} is the 4-wavenumber of the plane wave; finally, $\varepsilon_{\mu} k^{\mu} = 0$ reflects the gauge condition.

Considering the radiation scattered by the accelerating electron, we have

$$\frac{d^2N}{dq d\Omega} = \frac{\alpha}{4\pi^2 q} \left| \mathbf{q} \times \int_{-\infty}^{+\infty} \mathbf{u}(\tau) \exp[-iq_\mu x^\mu(\tau)] d\tau \right|^2, \quad (3)$$

where α is the fine structure constant, q_μ is the scattered 4-wavenumber, and $x_\mu(\tau)$ is the electron 4-position, which can be obtained by integrating the 4-velocity, after changing variables:

$$\begin{aligned} \frac{dx_\mu}{d\phi} &= \frac{dx_\mu}{d\tau} \frac{d\tau}{d\phi} = \frac{u_\mu}{d\phi/d\tau} = \frac{u_\mu}{k_\nu u_\nu^0} = \frac{u_\mu}{k_\nu u_\nu^0}; \\ x_\mu(\phi) &= x_\mu^0 + \frac{1}{k_\nu u_\nu^0} \int_0^\phi u_\mu d\psi. \end{aligned} \quad (4)$$

Using the invariance of the light-cone variable, and the definitions given above, the nonlinear electron 4-velocity and 4-position are:

$$\begin{aligned} u_\mu &= u_\mu^0 + \varepsilon_\mu A_0 \sin\phi - \frac{k_\mu}{2u_\nu^0 k^\nu} \left[\frac{A_0^2}{2} (1 - \cos 2\phi) + 2u_\nu^0 \varepsilon^\nu A_0 \sin\phi \right], \\ x_\mu &= x_\mu^0 + \frac{1}{u_\nu^0 k^\nu} \left[\left(u_\mu^0 - \frac{k_\mu}{2u_\nu^0 k^\nu} \frac{A_0^2}{2} \right) \phi + A_0 \cos\phi \left(\frac{u_\nu^0 \varepsilon^\nu}{u_\nu^0 k^\nu} \varepsilon_\mu - k_\mu \right) + \frac{k_\mu}{2u_\nu^0 k^\nu} \frac{A_0^2}{2} \frac{1}{2} \sin 2\phi \right]. \end{aligned} \quad (5)$$

At this point, it is crucial to note the intrinsic dc component in the nonlinear 4-velocity: $\sin^2 \phi = \frac{1}{2}(1 - \cos 2\phi)$; the constant term corresponds to the non-zero average of the 2nd harmonic motion over one period and is directly related with the dressed electron mass term in nonlinear Compton scattering.

Contracting Eq. (5) with the scattered 4-wavenumber leads to the nonlinear phase in the radiation formula:

$$q^\mu x_\mu = q^\mu x_\mu^0 + \frac{q^\mu}{u_\nu^0 k^\nu} \left[\left(u_\mu^0 - \frac{k_\mu}{2u_\nu^0 k^\nu} \langle A_\nu A^\nu \rangle \right) \phi + A_0 \cos \phi \left(\frac{u_\nu^0 \varepsilon^\nu}{u_\nu^0 k^\nu} \varepsilon_\mu - k_\mu \right) + \frac{k_\mu}{4u_\nu^0 k^\nu} \langle A_\nu A^\nu \rangle \sin 2\phi \right]; \quad (6)$$

The first term corresponds to the coherence factor in the case of multiple electrons, leading to a factor $\left| \sum_i e^{iq_\mu x_{0i}^\mu} \right|^2$. The remainder of the formula can be understood by examining its periodicity: the first and second harmonic terms are clearly periodic in ϕ ; the term that varies linearly with phase becomes periodic if the following resonance condition is satisfied:

$$\frac{q_n^\mu}{u_\nu^0 k^\nu} \left(u_\mu^0 - \frac{k_\mu}{2u_\nu^0 k^\nu} \langle A_\nu A^\nu \rangle \right) = n. \quad (7)$$

This condition defines a series of harmonic; introducing the direction of observation, defined such that $q_\mu = q(1, \mathbf{n})$, and using 3-vectors, Eq. (7) can be solved to obtain:

$$q_n = n \frac{\gamma_0 k - \mathbf{u}_0 \cdot \mathbf{k}}{\gamma_0 - \mathbf{u}_0 \cdot \mathbf{n} - \frac{A_0^2}{4} \left(\frac{k - \mathbf{k} \cdot \mathbf{n}}{\gamma_0 k - \mathbf{u}_0 \cdot \mathbf{k}} \right)}. \quad (8)$$

The relativistic Doppler upshift appears clearly, along with the radiation pressure-induced downshift; for example, in the case of head-on collisions, and observing the radiation scattered in the direction of the electron, one would find a series of harmonics defined by the fundamental frequency:

$$q_1 = \frac{\gamma_0 + u_0}{(\gamma_0 - u_0) \left(1 + \frac{A_0^2}{2}\right)} \quad (9)$$

At this point, it is well worth comparing this result with the nonlinear multi-photon Compton formula; to this end, we first consider 4-momentum conservation:

$u_\mu + \tilde{\lambda}_C (k_\mu^1 + k_\mu^2 + \dots k_\mu^n) = v_\mu + \tilde{\lambda}_C q_\mu^n$; since we are considering coherent plane waves,

$k_\mu^1 = k_\mu^2 = \dots = k_\mu^n$; this leads to considerable simplification, with $v_\mu = u_\mu + \tilde{\lambda}_C (nk_\mu - q_\mu^n)$.

Taking the square of this expression, and accounting for the fact that $u_\mu u^\mu = v_\mu v^\mu = 1$,

and $k_\mu k^\mu = q_\mu^n q_n^\mu = 0$, we have:

$$u^\mu (nk_\mu - q_\mu^n) = \tilde{\lambda}_C nk_\mu q_n^\mu; \quad (10)$$

Now replacing u_μ by the nonlinear solution from Eq. (2), we have:

$$\begin{aligned}
& \left(u_{\mu}^0 + A_{\mu} - k_{\mu} \frac{A_{\nu} A^{\nu} + 2u_{\nu}^0 A^{\nu}}{2u_{\nu}^0 k^{\nu}} \right) (nk^{\mu} - q_n^{\mu}) = \tilde{\lambda}_c nk_{\mu} q_n^{\mu}; \\
& nu_{\mu}^0 k^{\mu} - \left(u_{\mu}^0 - \frac{k_{\mu}}{2u_{\nu}^0 k^{\nu}} \langle A_{\nu} A^{\nu} \rangle \right) q_n^{\mu} = \tilde{\lambda}_c nk_{\mu} q_n^{\mu}.
\end{aligned} \tag{11}$$

The second equality is obtained by considering the invariance of the light-cone variable, which derives from the gauge condition, $k_{\mu} A^{\mu} = 0$, and the dispersion relation, $k_{\mu} k^{\mu} = 0$, and by taking the average over one cycle, with $\langle f \rangle = \frac{1}{2\pi} \int_0^{2\pi} f(\phi) d\phi$. Taking the classical limit, where $\tilde{\lambda}_c \rightarrow 0$, which eliminates recoil, we recover the nonlinear Thomson scattering harmonics of Eq. (7). This clearly establishes the connection between harmonics and multi-photon effects.

Even in the linear regime, the Thomson and Compton scattering formalisms yield different radiation frequencies:

$$\begin{aligned}
\omega_1 &= \omega_0 \frac{\gamma + u}{\gamma - u + 2(\hbar\omega_0 / m_0 c^2)}, \\
\omega_2 &= \omega_0 \frac{\gamma + u}{\gamma - u}, \\
\Delta &= 2 \frac{\omega_2 - \omega_1}{\omega_2 + \omega_1} = \frac{2(\hbar\omega_0 / m_0 c^2)}{\gamma - u + (\hbar\omega_0 / m_0 c^2)}.
\end{aligned} \tag{12}$$

The relative difference is plotted in Fig. 1, as a function of the electron energy, for a 1,064 nm laser, head-on collisions, and on-axis scattering. For NRF, a relative difference of 10^{-6} is comparable to the Doppler-broadened line width; therefore, models

require this level of accuracy for such applications. It is interesting to note that the introduction of a simple term in the classical electron trajectory can yield the correct frequency: modifying Equation (2), we have

$$u_\mu = u_\mu^0 + A_\mu - k_\mu \frac{A_\nu A^\nu + 2u_\nu^0 A^\nu}{2u_\nu^0 k^\nu} - \tilde{\lambda}_c k_\mu; \quad (13)$$

integrating over proper time to yield the modified ballistic trajectory and introducing the new electron phase in the radiation formula,

$$\frac{d^2 N}{dq d\Omega} = \frac{\alpha}{4\pi^2 q} \left| \frac{\mathbf{q}}{k_\mu u_0^\mu} \times \left(\mathbf{A}_0 + \mathbf{k} \frac{\mathbf{A}_0 \cdot \mathbf{u}_0}{k_\mu u_0^\mu} \right) e^{-iq_\mu x_0^\mu} \int_{-\infty}^{+\infty} \exp \left\{ -i\phi \left[1 - \frac{q_\mu (u_0^\mu - \tilde{\lambda}_c k^\mu)}{k_\mu u_0^\mu} \right] \right\} d\phi \right|^2. \quad (14)$$

The delta-function resonance now clearly contains the correct recoil term.

We now turn our attention to the Klein-Nishina differential scattering cross-section; in QED units, the covariant, spin-independent expression reads [5]:

$$\frac{d\sigma}{d\Omega} = \frac{\alpha^2}{2} \left(\frac{q}{\kappa} \right)^2 \left\{ \frac{1}{2} \left(\frac{\kappa}{\lambda} + \frac{\lambda}{\kappa} \right) - 1 + 2 \left[\varepsilon_\mu \pi^\mu - \frac{(\varepsilon_\mu u^\mu)(\pi_\mu v^\mu)}{\kappa} + \frac{(\varepsilon_\mu v^\mu)(\pi_\mu u^\mu)}{\lambda} \right]^2 \right\}, \quad (15)$$

where $\kappa = u_\mu k^\mu$ and $\lambda = u_\mu q^\mu$ are the incident and scattered light-cone variables [11]; ε_μ and π_μ are the incident and scattered polarizations; $v_\mu = u_\mu + k_\mu - q_\mu$ is the scattered

electron 4-velocity. For large values of the recoil parameter, $k\lambda_c$, the cross-section, observed in the initial electron frame deviates from the conventional dipole, as illustrated in Fig. 2; this is due to the kinematics of the elastic collision.

The differential brightness approach is now described in broad terms; the key quantity is:

$$\frac{d^{12}N}{d\Omega dq d^4x_\nu d^3u_i d^3k_j} = \frac{d\sigma}{d\Omega} \delta [q_\mu (u^\mu + k^\mu) - k_\mu u^\mu] j_\mu(x_\nu, u_\nu) \Phi^\mu(x_\nu, k_\nu). \quad (16)$$

The electron 4-current phase space density is:

$$j_\mu = u_\mu (d^6n_e / d^3x_i d^3u_i) = \eta_e u_\mu. \quad (17)$$

The incident photon 4-flux phase space density is:

$$\Phi_\mu = k_\mu (d^6n_\lambda / d^3x_i d^3k_j) = \eta_\lambda k_\mu. \quad (18)$$

Integration over all phase space yields the number of photons scattered per unit solid angle, frequency, detector time, and surface area:

$$\frac{d^5N}{d\Omega dq dt_d dx dy} = \int_{\square} \frac{d\sigma}{d\Omega} \delta \left[q_\mu (u^\mu + k^\mu) - k_\mu u^\mu \right] \delta \left[t_d - \left(t - q \frac{\mathbf{x} \cdot \mathbf{n}_d}{\mathbf{q} \cdot \mathbf{n}_d} \right) \right] j_\mu(x_v, u_v) \Phi^\mu(x_v, k_v) dz dt d^3 u_i d^3 k_i. \quad (19)$$

In special cases, such as narrow-band, transform-limited laser pulses, the incident photon phase space is uncorrelated, and relatively easily described; however, more complex situations require in-depth analysis, which can be approached within the context of the Wigner distribution function [8] and the formalism introduced by Oliveira e Silva and Mendonça [9].

In Figures 3-6, an example is given, where a 1 J, 532 nm, 10 ps FTL laser pulse interacts with a 250 MeV, 1 nC, 0.64 mm.mrad normalized emittance, 3.2 ps electron bunch focused in a 20 μm spot; the predicted dose is 3×10^8 photons/shot. In this specific case, $A_0^2 = 0.000659$, and a linear theory is adequate; however, recoil plays a role, and is taken into account since the application for this source is NRF.

4. Conclusions

A brief overview of Compton scattering in the linear and nonlinear regimes has been presented, with a special emphasis on the different models used to describe the interaction, and some considerations on the physical mechanisms underlying the nonlinear regime. A comparison between Thomson and Compton scattering has also been given, along with arguments indicating the need to account for recoil for precision applications, such as NRF.

Acknowledgements

This work performed under the auspices of the U.S. Department of Energy by Lawrence Livermore National Laboratory under Contract DE-AC52-07NA27344. The author also wishes to acknowledge important discussions with A.K. Kerman, D.T. Santa Maria, and R. Hauptman.

References

- [1] A.H. Compton, Phys. Rev. 21, 483 (1923).
- [2] W.J. Brown and F.V. Hartemann, Phys. Rev. STAB 7, 060703 (2004).
- [3] W.J. Brown *et al.*, Phys. Rev. STAB 7, 060702 (2004).
- [4] F.V. Hartemann *et al.*, Phys. Rev. STAB 8, 100702 (2005).
- [5] G. Bhatt *et al.*, Phys. Rev. A 28, 2195 (1983).
- [6] J. Pruet *et al.*, J. App. Phys. 99, 123102 (2006).
- [7] F.V. Hartemann *et al.*, Phys. Rev. E 64, 016501 (2001).
- [8] E. Wigner, Phys. Rev. 40, 749 (1932).
- [9] L. Oliveira e Silva and J.T. Mendonça, Phys. Rev. E 57, 3423 (1998).
- [10] J.D. Jackson, Classical Electrodynamics, third ed., Wiley, New York, 1998.
- [11] L.M. Brown and R.P. Feynman, Phys. Rev. 85, 231 (1952).

Figure captions

Fig. 1 Relative difference between the Compton and Thomson scattering frequencies for head-on collisions, 1,064 nm laser wavelength, on-axis radiation, as a function of γ .

Fig. 2 Compton scattering differential cross-section in the linear regime, in the initial rest frame of the electron for 3 values of the recoil parameter: $k\lambda_c = 0, 0.5,$ and 1.0 (From left to right) .

Fig. 3 250 MeV, 0.64 mm.mrad normalized emittance, 3.2 ps electron bunch phase space, as modeled by Parmela. Top: transverse macro-particle distribution at focus. Bottom: $x - u_x$ distribution at focus.

Fig. 4 Source size (green Parmela, blue super-Gaussian fit, red Gaussian laser profile).

Fig. 5 Spectrum and angular correlation.

Fig. 6 Radiation pattern and spectrum. The shape of the top radiation pattern results from the fact that the polarization is along the vertical axis; the projection of the dipole pattern results in the quasi-elliptical shape.

Fig. 1

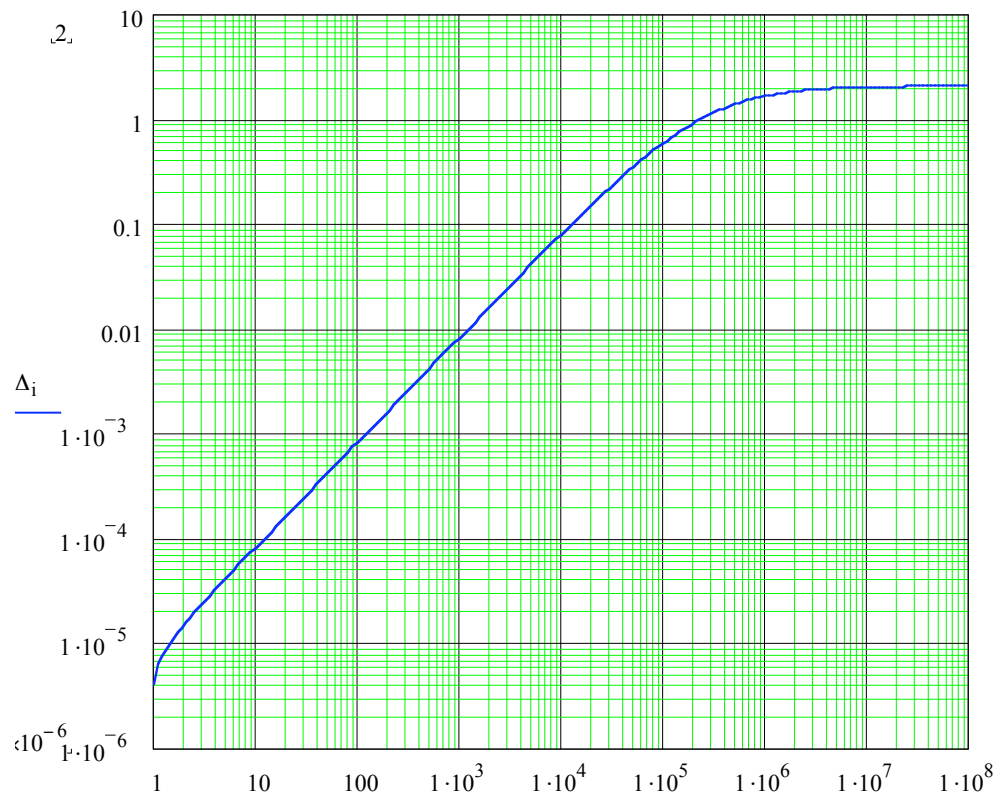


Fig. 2

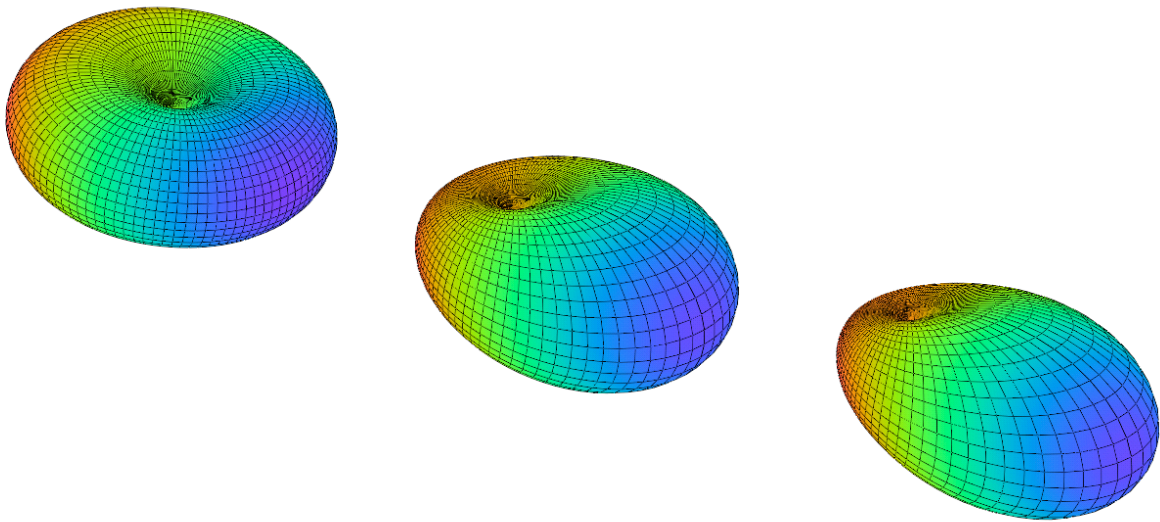


Fig. 3

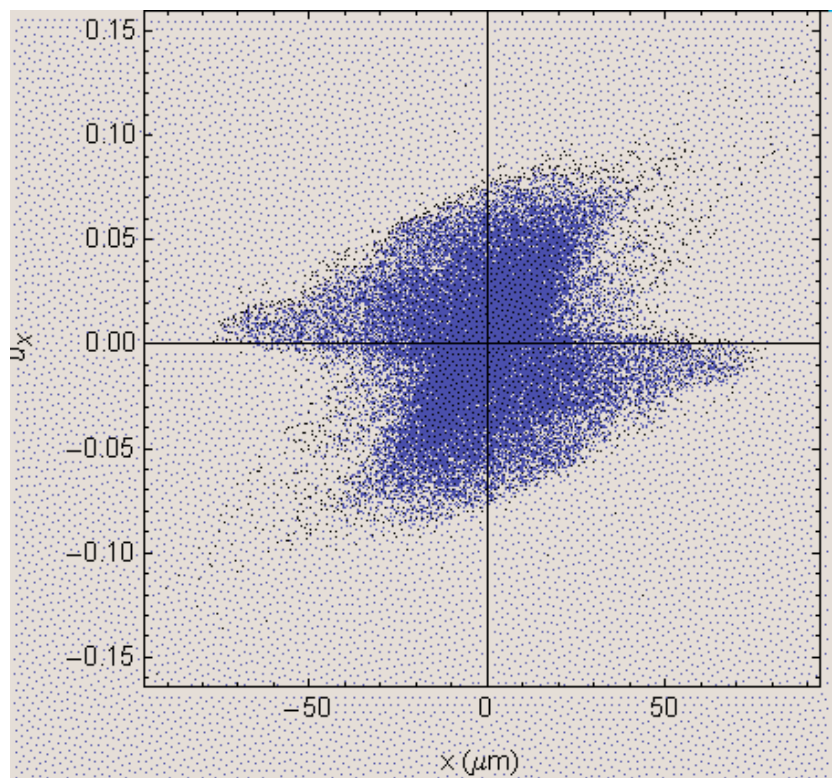
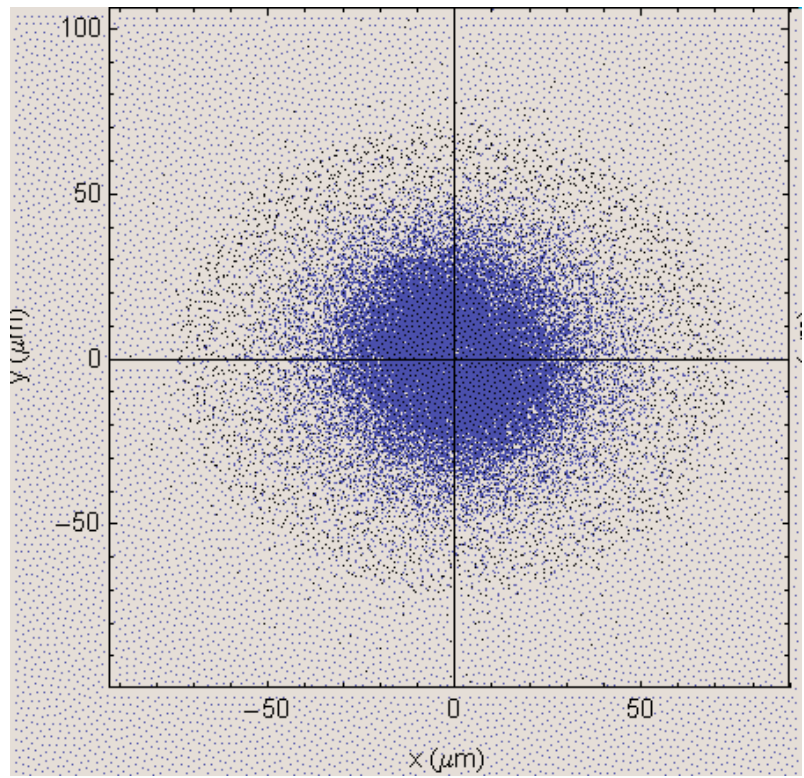


Fig. 4

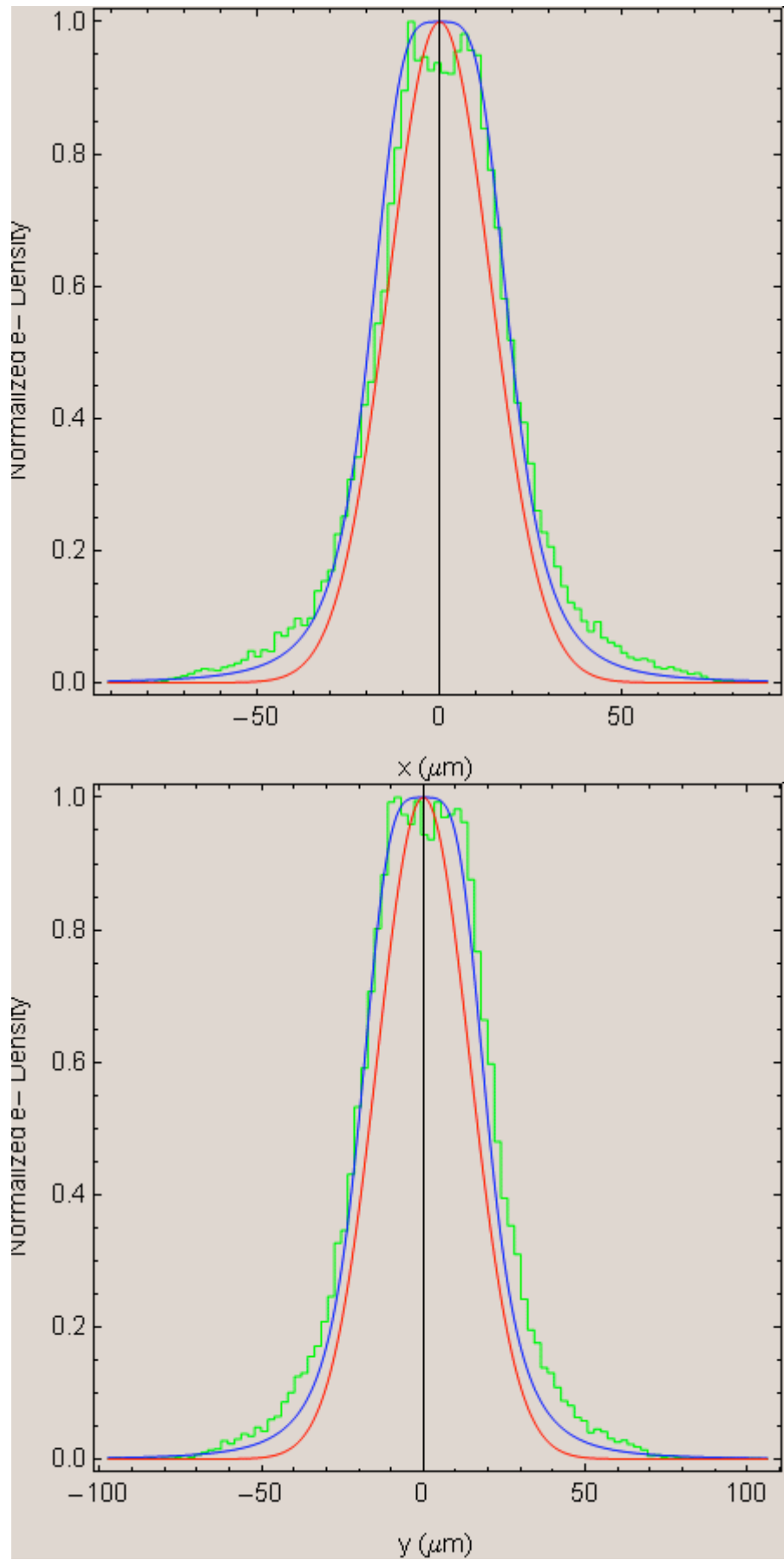


Fig. 5

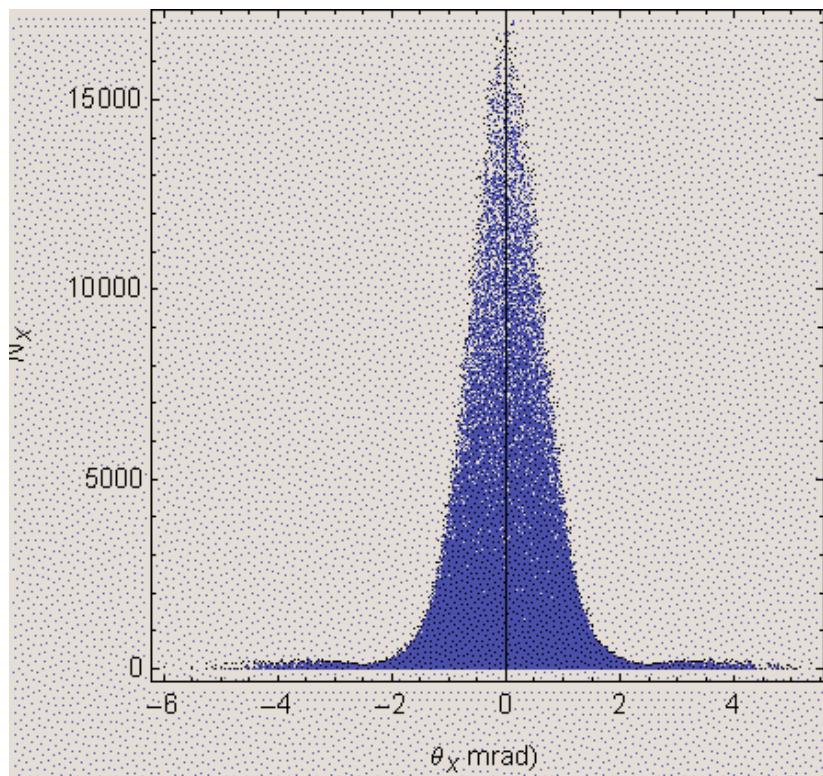
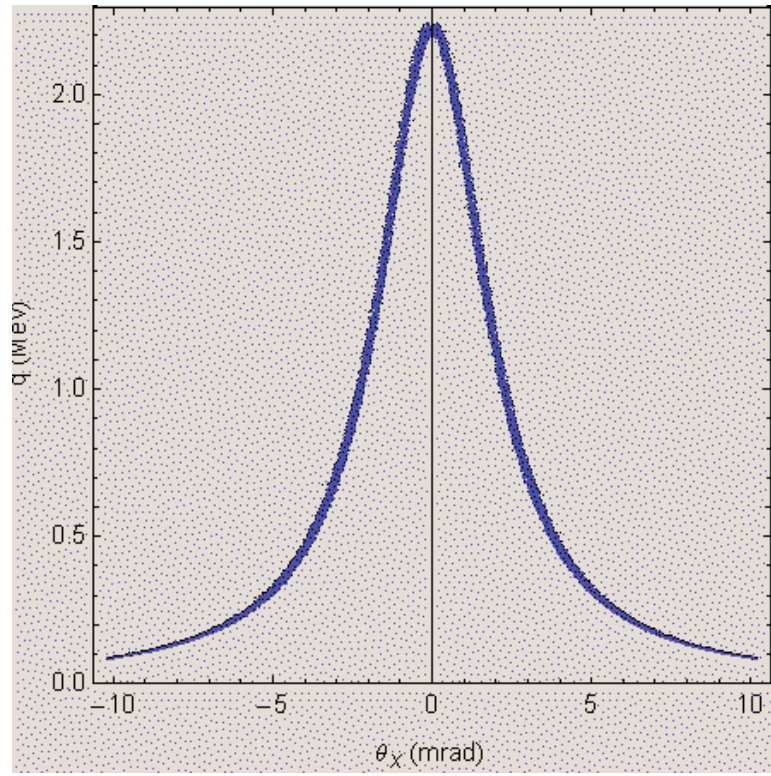


Fig. 6

